

Supplemental Information: Design Principles from Glass Sponges for Structurally Robust Lattices

**MATHEUS C. FERNANDES¹, JAMES C. WEAVER², JOANNA AIZENBERG^{1,2,3}, AND
KATIA BERTOLDI^{1,2,3,*}**

¹John A. Paulson School of Engineering and Applied Sciences – Harvard University, Cambridge, MA 02138

²Wyss Institute – Harvard University, Cambridge, MA 02138

³Kavli Institute – Harvard University, Cambridge, MA 02138

* Corresponding author: bertoldi@seas.harvard.edu

Compiled October 22, 2018

1.1. STRUCTURE OF THE HEXACTINELLID SPONGE *EUPLECTELLA ASPERGILLUM*

2 The periodic structures investigated in this study are inspired by the skeleton of the Hexactinellid sponge *Euplectella aspergillum* (sp.), commonly known as the "Venus' flower basket". In this section we provide a detailed description of the 4 sponge geometry and measured dimensions.

5 [Figure S1](#) shows a photograph of the entire skeleton of the *Euplectella* sp., and its intricate, cylindrical cage-like structure 6 (20 to 25cm long, 2 to 4 cm in diameter) ([Aizenberg et al., 2005](#)). The surface of the cylinder consists of a regular square 7 lattice composed of a series of cemented vertical and horizontal struts with circular cross-section. The cell spacing 8 between horizontal and vertical struts was reported to be $L \approx 2.5\text{mm}$ ([Weaver et al., 2007](#)), while their diameter was 9 measured to be $D_{nd} \approx 0.25\text{mm}$ ([Weaver et al., 2007](#)). Besides the horizontal and vertical struts, there is an additional 10 set of diagonal elements, intersecting in a manner that creates a series of alternating open and closed cells, reminiscent 11 of a checkerboard pattern ([Weaver et al., 2007](#)). Although these diagonal elements are not as ordered as the horizontal 12 and vertical ones, it has been shown that they can be approximated with two diagonal struts that are offset from the 13 nodes (vertex joints between non-diagonal elements) and form octagonal openings ([fig. S1\(d\)](#)). To estimate the volume 14 ratio between diagonal and non-diagonal elements, we took high resolution photographs of the sponge and performed 15 image segmentation to segregate the projected area of the vertical/horizontal and diagonal spicules. Using this approach, 16 the projected area ratio of non-diagonal to diagonal elements was found to be $A_{nd}/A_d \approx 1.4$. Note that here, and in the 17 following, the subscripts *d* and *nd* are used to indicate diagonal and non-diagonal (i.e. horizontal and vertical) elements, 18 respectively.

19 Finally, it should also be noted that the sponge is reinforced by external ridges that extend perpendicular to the surface 20 of the cylinder and spiral the cage at an angle of 45°. However, in this paper we do not report the effects of these ridges 21 on its structural performance.

2.1.1. Image Segmentation Analysis

23 →@James, add details of image segmentation analysis performed for extracting diameter ratios between diagonals
24 and non-diagonals

2. OUR FOUR DESIGNS

26 In this study, we focus on four different lattice configurations (Designs A, B, C and D) constrained to deform in an 27 in-plane setting only. In an effort to conduct a fair performance comparison between the different designs, all four 28 designs are characterized by the same total volume of material and a fixed volume ratio between non-diagonal and 29 diagonal elements (chosen to match the sponge geometry). Two different shapes are considered for the cross-section of 30 the struts: circular and rectangular. For the circular cross-section case we denote the diameters with $D_{\alpha,nd}$ and $D_{\alpha,d}$ of the 31 non-diagonal (i.e. horizontal and vertical) and diagonal struts in the α -th design, respectively, and neglect out-of-plane 32 buckling. For the rectangular cross-sections we choose the depth H and in-plane thickness $T_{\alpha,nd}$ and $T_{\alpha,d}$ to avoid 33 out-of-plane deformation (i.e. we choose the depth over thickness ratio sufficiently large). Finally, it is important to note 34 that the slenderness of the non-diagonal members in the α -th design $\in [A, B, C]$ is chosen as

$$\frac{D_{\alpha,nd}}{L} = 0.1, \quad \text{and} \quad \frac{T_{\alpha,nd}}{L} = 0.1, \quad (1)$$

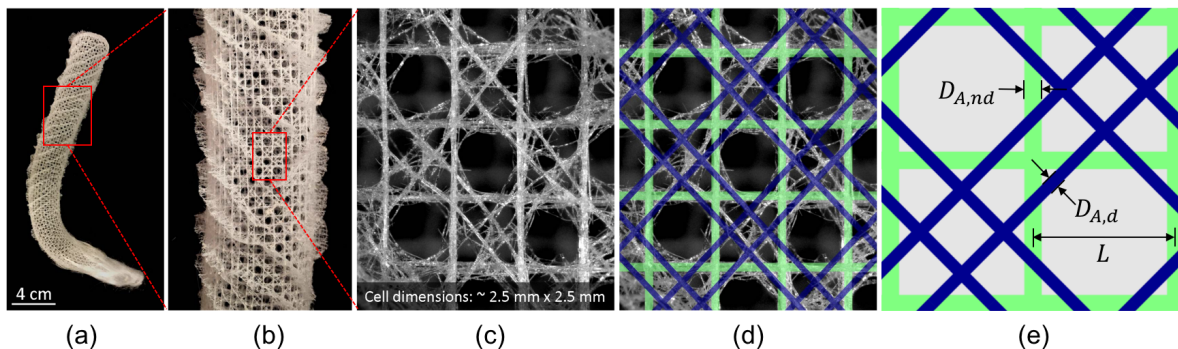


Figure S1: Hexactinellid sponge *Euplectella aspergillum*. (a)-(b) Full-frame photo of sponge. (c) Close up microscope image of the sponge. (d) Comparison between the idealized model (green and blue lines) and the sponge structure. (e) Unit cell of the idealized model.

35 for the case of circular and rectangular cross section, since this is the aspect ratio measured for the sponges (see [section 1](#)).
 36 In the subsequent sections, we describe in detail the unit cells for four different designs, and provide the derivations
 37 for each geometry cross-section characteristics.

38 2.1. Design A

39 Design A is inspired by the sponge structure and consists of a square grid reinforced by a double diagonal system
 40 (see [fig. S2](#)). As for the case of the sponge, the diagonal elements are assumed to form an octagonal opening on every
 41 other cell, so that they intersect the horizontal and vertical struts at a distance $\Delta L = L/(\sqrt{2} + 2)$ from the nodes, where L
 42 denote the length of the vertical/horizontal struts.

43 2.1.1. Circular cross section

44 If we assume that cross section of all struts is circular, the projected area and volume for the non-diagonal ($A_{A,nd}$ and
 45 $V_{A,nd}$) and diagonal ($A_{A,d}$ and $V_{A,d}$) members is given by

$$46 \quad A_{A,nd} = 8LD_{A,nd}, \quad (2)$$

$$47 \quad V_{A,nd} = 8L \left(\pi \frac{D_{A,nd}^2}{4} \right) = 2L\pi D_{A,nd}^2 \quad (3)$$

$$48 \quad A_{A,d} = 8\sqrt{2}LD_{A,d}, \quad (4)$$

48 and

$$49 \quad V_{A,d} = 8\sqrt{2}L \left(\pi \frac{D_{A,d}^2}{4} \right) = 2\sqrt{2}L\pi D_{A,d}^2. \quad (5)$$

50 Since the projected area ratio of the non-diagonal to diagonal elements in the sponge has been measured to be

$$51 \quad \frac{A_{A,nd}}{A_{A,d}} = 1.4, \quad (6)$$

52 by substituting [eq. \(2\)](#) and [eq. \(4\)](#) into the equation above we find that for Design A

$$53 \quad D_{A,nd} = 1.4\sqrt{2}D_{A,d} \approx 2D_{A,d}. \quad (7)$$

54 Substitution of [eq. \(7\)](#) into [eq. \(3\)](#) and [eq. \(5\)](#) yields

$$55 \quad \frac{V_{A,nd}}{V_{A,d}} = \frac{2L\pi D_{A,nd}^2}{2\sqrt{2}L\pi D_{A,d}^2} = 2\sqrt{2} \quad (8)$$

56 and

$$57 \quad V_{A,T} = V_{A,nd} + V_{A,d} = 2\pi L(D_{A,nd}^2 + \sqrt{2}D_{A,d}^2) = 2\pi LD_{A,nd}^2 \left(1 + \frac{1}{2\sqrt{2}} \right), \quad (9)$$

53 where $V_{A,T}$ indicates the total volume of the unit cell for Design A.

54 Finally, it is important to note that in this study we use Design A as our base model, and thus constrain the total
55 volume of all the other unit cell designs with circular cross section to be equal to that of Design A, namely,

$$V_{\alpha,d} + V_{\alpha,nd} = V_{A,T} = 2\pi LD_{A,nd}^2 \left(1 + \frac{1}{2\sqrt{2}}\right), \quad (10)$$

56 with $\alpha = B, C$ and D. For Designs B and C, which comprise diagonal elements, we also constrain the volume ratio of the
57 non-diagonal to diagonal elements to be the same as in Design A

$$\frac{V_{\alpha,nd}}{V_{\alpha,d}} = \frac{V_{A,nd}}{V_{A,d}} = 2\sqrt{2}, \quad (11)$$

58 with $\alpha \in B$ and C.

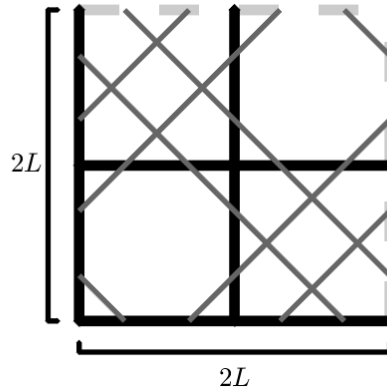


Figure S2: Unit cell for Design A. This design is inspired by the sponge structure and consists of a square grid reinforced by a double diagonal system. The horizontal and vertical struts have length L and circular cross section with diameter $D_{A,nd}$ and, as with the sponge, we assume $D_{A,nd}/L = 0.1$. The diagonal elements have a circular cross section with diameter $D_{A,d} = 2D_{A,nd}$.

59 2.1.2. Rectangular cross-section

60 If we assume that the cross section of all struts is rectangular, the projected-area for the non-diagonal ($A_{A,nd}$) and
61 diagonal ($A_{A,d}$) members is given by

$$A_{A,nd} = 8LT_{A,nd} \quad (12)$$

62 and

$$A_{A,d} = 8\sqrt{2}LT_{A,d} \quad (13)$$

63 where $T_{A,nd}$ and $T_{A,d}$ are the non-diagonal and diagonal in-plane strut thickness for Design A, respectively. Since for the
64 sponge $A_{nd}/A_d \approx 1.4$, it follows that

$$T_{A,nd} = 2T_{A,d}. \quad (14)$$

65 Finally, also for the case of rectangular cross-section we use Design A as our base model, and thus constrain the total
66 volume of all the other unit cell designs with rectangular cross-section to be equal to that of Design A, namely,

$$V_{A,T} = V_{\alpha,d} + V_{\alpha,nd} = 8LH(T_{A,nd} + \sqrt{2}T_{A,d}) = 8LHT_{A,nd} \left(1 + \frac{1}{\sqrt{2}}\right), \quad (15)$$

67 with $\alpha \in B, C$ and D. Moreover, for Designs B and C, which comprise diagonal elements, we also constrain the volume
68 ratio of the non-diagonal to diagonal elements to be the same as in Design A,

$$\frac{V_{\alpha,nd}}{V_{\alpha,d}} = \sqrt{2}, \quad (16)$$

69 with $\alpha \in B$ and C.

70 2.2. Design B

71 Design B is similar to the sponge design (Design A) and is likewise characterized by an alternation of open and closed
72 cells (fig. S3). However, instead of having two diagonals offset from the nodes, here we only have one diagonal passing
73 through the nodes and crossing every other cell.

74 2.2.1. Circular cross section

75 For this design with circular cross section the non-diagonal and diagonal volumes are given by

$$V_{B,nd} = V_{A,nd} = 2\pi L D_{B,nd}^2 \quad (17)$$

76 and

$$V_{B,d} = 2\sqrt{8}L \left(\pi \frac{D_{B,d}^2}{4} \right), \quad (18)$$

77 respectively. Using the constraints provided by [eq. \(10\)](#) and [eq. \(11\)](#), as well as the above volumes, we obtain

$$D_{B,nd} = D_{A,nd} \quad (19)$$

78 and

$$\frac{D_{B,d}}{D_{B,nd}} = \frac{1}{\sqrt{2}}. \quad (20)$$

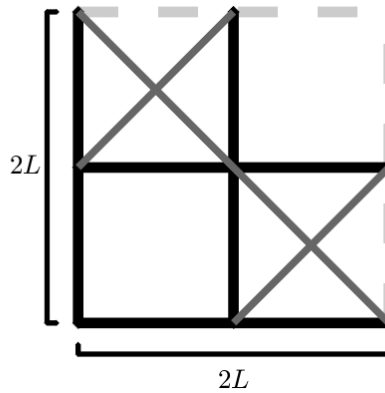


Figure S3: Unit cell for Design B. This design is still characterized by an alternation of open and closed cells. However, instead of having two diagonals offset from the nodes, here we only have one diagonal passing through the nodes and crossing every other cell. The horizontal and vertical struts have length L and a circular cross section with diameter $D_{B,nd}$. The diagonal elements have a circular cross section with diameter $D_{B,d} = D_{B,nd}/\sqrt{2}$.

79 2.2.2. Rectangular cross section

80 For this design with circular cross section the volume of the non-diagonal and diagonal members are given by

$$V_{B,nd} = 8LT_{B,nd}H. \quad (21)$$

81 and

$$V_{B,d} = 4\sqrt{2}LT_{B,d}H. \quad (22)$$

82 Using the constraints provided by [eq. \(15\)](#) and [eq. \(16\)](#), as well as the above volumes, we obtain

$$T_{B,nd} = T_{B,d} \quad (23)$$

83 and

$$T_{B,nd} = T_{A,nd} \quad (24)$$

84 2.3. Design C

85 Design C is inspired by the town lattice truss design introduced by architect Ithiel Town in 1820 ([Waddell, 1916](#)) and **86** consists of every cell being reinforced by diagonal trusses passing through the nodes (see [fig. S4](#)).

87 2.3.1. Circular cross section

88 For this design with circular cross section, the volume of the non-diagonal and diagonal members of the unit cell are
 89 given by:

$$V_{C,nd} = V_{A,nd} = 2L\pi D_{A,nd}^2 \quad (25)$$

90 and

$$V_{C,d} = V_{A,d} = 2\sqrt{2}L\pi D_{A,d}^2, \quad (26)$$

91 respectively. Using the constraints provided by eq. (10) and eq. (11) we obtain

$$D_{C,nd} = D_{A,nd} \quad (27)$$

92 and

$$\frac{D_{C,d}}{D_{C,nd}} = \frac{1}{2}. \quad (28)$$

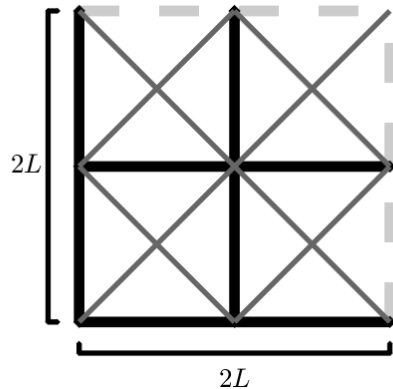


Figure S4: Unit cell for Design C. This design consists of a square grid with all cells being reinforced by diagonal trusses passing through the nodes. The horizontal and vertical struts have length L and a circular cross section with diameter $D_{C,nd}$. The diagonal elements have a circular cross section with diameter $D_{C,d} = D_{C,nd}/2$.

93 2.3.2. Rectangular cross section

94 For this design with circular cross section, the volume of the non-diagonal and diagonal members of the unit cell are
 95 given by

$$V_{C,nd} = 8LT_{C,nd}H \quad (29)$$

96 and

$$V_{C,d} = 8\sqrt{2}LT_{C,d}H \quad (30)$$

97 Using the constraints provided by eq. (15) and eq. (16), as well as the above volumes, we obtain

$$T_{C,nd} = 2T_{C,d}, \quad (31)$$

98 and

$$T_{C,nd} = T_{A,nd}. \quad (32)$$

99 2.4. Design D

100 Design D comprises only the square grid without diagonal reinforcement (fig. S5). As such, for this design we allocate
 101 the total material volume to the non-diagonal elements. Note that this design is well known to be unstable and very
 102 limited in resisting shear forces (Gibson and Ashby, 1999; Deshpande et al., 2001).

103 2.4.1. Circular cross section

104 Since

$$V_{D,T} = V_{D,nd} = V_{A,nd} = 2\pi LD_{D,nd}^2, \quad (33)$$

105 using the constraint provided by eq. (10) we obtain

$$D_{D,nd} = D_{A,nd} \sqrt{1 + \frac{\sqrt{2}}{4}}. \quad (34)$$

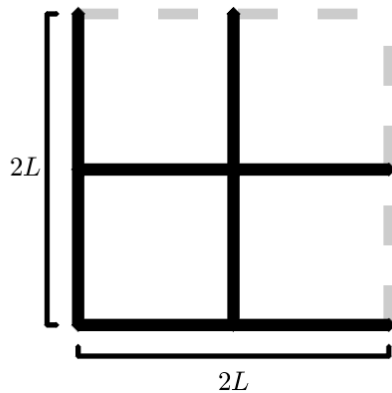


Figure S5: Unit cell for Design D. This design consists of a square grid without diagonal reinforcement. The horizontal and vertical struts have length L and a circular cross section with diameter $D_{D,nd}$.

106 2.4.2. Rectangular cross-section

107 Since

$$V_{D,T} = V_{D,nd} = 8LT_{D,nd}H, \quad (35)$$

108 using the constraint provided by eq. (15) we obtain

$$T_{D,nd} = \left(1 + \frac{1}{\sqrt{2}}\right) T_{A,nd} \quad (36)$$

109 3. NUMERICAL MODEL

110 The finite element analysis presented in this article were conducted using the *ABAQUS/Standard*. All models were
111 constructed using 1D Timoshenko beam (ABAQUS element type B22) and all beam crossings were assumed to be welded
112 joints. For each instance, seeding of the mesh was chosen to be at least 1/10 of the minimum beam length. The response
113 of the material was captured using a linear elastic model with Poisson's ratio $\nu = 0.3$ and Young's modulus of E .

114 To reduce the computational cost, we took advantage of the periodicity of the structures and investigated their
115 response using the unit cells shown in fig. S6. To subject the unit cells to a macroscopic deformation gradient $\bar{\mathbf{F}}$ periodic
116 boundary conditions are imposed on all cell boundaries by enforcing (Danielsson et al., 2002; Bertoldi and Boyce, 2008)

$$\mathbf{u}_\alpha^{A_i} - \mathbf{u}_\alpha^{B_i} = (\bar{\mathbf{F}}_{\alpha\beta} - \delta_{\alpha\beta})(\mathbf{X}_\beta^{A_i} - \mathbf{X}_\beta^{B_i}), \quad i = 1, 2, \dots, K \quad (37)$$

117 where $\delta_{\alpha\beta}$ is the Kronecker delta, $\mathbf{u}_\alpha^{A_i}$ and $\mathbf{u}_\alpha^{B_i}$ ($\alpha = 1, 2$) are displacements of points periodically located on the boundary
118 of the unit cell. Moreover, K denotes the number of pairs of nodes periodically located on the boundary of the unit cell.
119 Note that the components of $\bar{\mathbf{F}}$ can be conveniently prescribed within the finite element framework using a set of virtual
120 nodes. The corresponding macroscopic first Piola-Kirchoff stress $\bar{\mathbf{P}}$ is then obtained through virtual work considerations
121 (Danielsson et al., 2002; Bertoldi and Boyce, 2008).

122 To subject the structures to uniaxial compression, in this study the following uniaxial macroscopic loading condition
123 was considered:

$$\bar{\mathbf{F}} = \begin{bmatrix} \text{UNSET} & 0 \\ 0 & \lambda_y \end{bmatrix} \quad (38)$$

124 In order to investigate the structure's buckling and elastic stiffness response in all directions, we rotate the unit cell
125 model by angle θ and re-apply the above periodic boundary conditions using the rotated geometry coordinates. This
126 approach allows us to rotate the base orthogonal coordinate system with respect to the unit cell.

127 To determine the initial stiffness of the structures we performed a linear elastic analysis. To calculate stiffness we use a
128 displacement controlled simulation and extract the total reaction force from the model. To obtain the structures response
129 to varying angle, we follow the simple procedure detailed in the previous paragraph to rotate the boundary condition.
130 Knowing the displacement applied and the total reaction force, we can use this information to compute the structural
131 stiffness.

132 For all buckling analysis, we performed a linear stability buckling analysis (*Buckling command in ABAQUS input
133 file). We perform this analysis for varying angles θ and extract the first mode critical buckling strain. Since buckling
134 may alter the periodicity of the structure, we considered super cells consisting of $M \times M$ undeformed RVEs subjected to

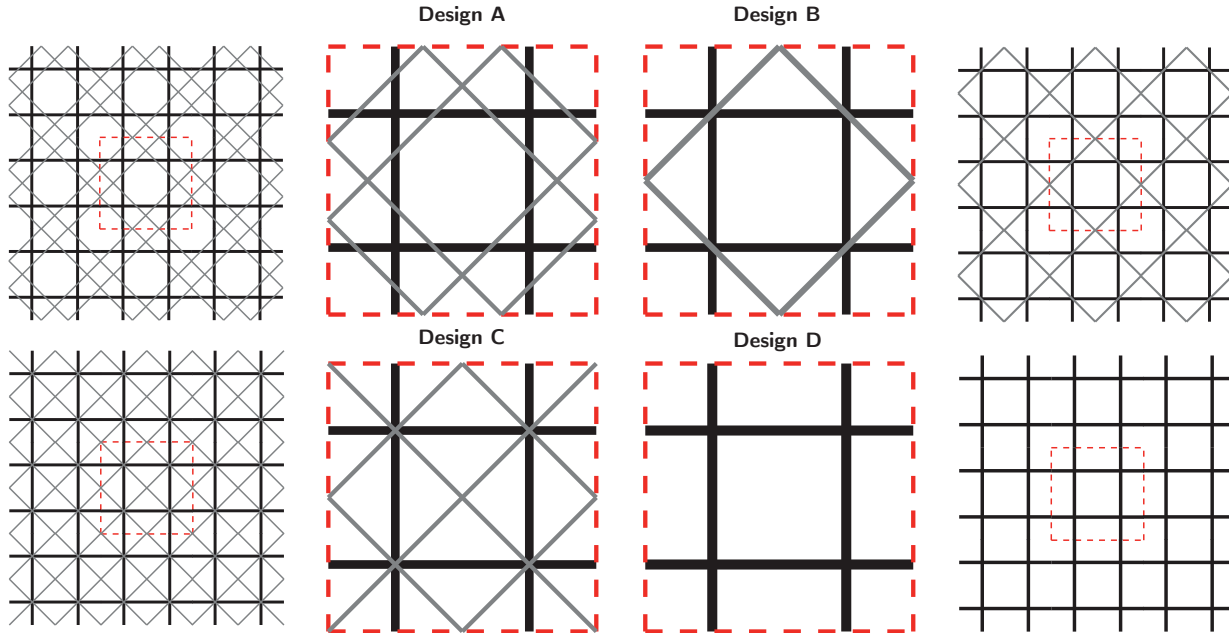


Figure S6: RVE used for the different designs. This figure portrays the different RVEs used for the different designs considered. Each unit cell is shifted by half of a square cell to the horizontally and half of a square cell vertically. Periodic boundary conditions are applied on the nodes that intersect with the light gray dashed line.

135 periodic boundary conditions and calculated the critical strain for each of them. The critical strain of the infinite periodic
 136 structure is then defined as the minimum critical strain on all considered super cells. See fig. S12 for this detailed analysis.
 137 From the main article figure## [→ add reference to main article results figure](#) we conclude that for all θ , Design
 138 A provides a higher overall buckling strength over the other compared designs, while not compromising its overall
 139 stiffness in every direction.

140 4. EXPERIMENTAL SETUP

141 [→ add full description of experimental setup and full table of 3D printed material properties; @James: I need to material](#)
 142 [properties](#)

143 5. OPTIMIZATION ANALYSIS

144 In an effort to identify lattice configurations resulting in large critical loads, we used a Python implementation of
 145 the Covariance Matrix Adaptation Evolution Strategy (CMA-ES) (Hansen et al., 2003). CMA-ES is an evolutionary
 146 algorithm that is used to solve optimization/inverse problems by iteratively solving several forward problems to adjust
 147 a covariance matrix of the solution. CMA-ES is a derivative free algorithm, well suited for optimization problems of high
 148 dimensionality and non-linear parameter topology.

149 In this study we used CMA-ES to identify

- 150 • the number of diagonals, N
- 151 • the volume ratio of non-diagonal to diagonal members, $\lambda = V_{nd} / V_d$.
- 152 • the separation between each even set of diagonals, S_i (see Fig. S7)

153 resulting in a lattice structure with the large critical load. For such optimization problem, the number of optimization
 154 variables increases with the number of diagonals incorporated in the model (i.e. the total number of parameters are
 155 $1 + \frac{1}{2}(N - (N \bmod 2))$ for a given optimization instance with N number of diagonals). Note, for simulations with odd
 156 number of diagonal reinforcements, only an even number of diagonals are separated while keeping one diagonal going
 157 through the non-diagonal junction in order to ensure geometry symmetry (see Fig. S7).

158 The algorithm's initial values are chosen to be in the center of the design space, namely, $\lambda = 1$ and diagonal separation
 159 for the even set of diagonals $S_i = 0.5 * L$. The covariance matrix is initialized uniformly with standard deviation (σ) half
 160 of the domain space, which are normalized to remain between 0 and 1. The optimization is run for uniaxial loading
 161 condition in the direction parallel to the vertical elements.

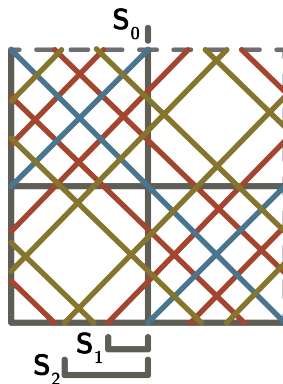


Figure S7: Schematic depicting parameters of Optimization. This schematic shows an example optimization geometry at a complexity level of five diagonals. For each set of even diagonals, we allow each diagonal to travel away from each other from the center junction with distances S_1, S_2 . Note that for every odd diagonal, the distance $S_0 = 0$ and it is not allowed to vary in order to ensure symmetry.

162 For the optimization results presented in the main article, we seek to maximize the critical buckling load using a single
163 objective target function. However, an equivalent analysis is performed to maximize the critical buckling strain as the
164 target response (fig. S8.)

165 ⇒ Add table with optimal parameters results for each N, for both circular and rectangular cross-sections

166 6. CIRCULAR CROSS-SECTION RESULTS

167 The results presented here complement that found on the main article and show that the structural benefit for the
168 Design A persists when using a different cross-section for the structure. We show that for varying loading angles all of
169 the diagonally reinforced designs provide the same stiffness, but Design A consistently provides the best resistance to
170 buckling.

171 7. PARAMETER EXPLORATION

172 In order to survey the design space of the double diagonal construction we explore parametric simulations for 2
173 variables: diagonal separation and mass ratio. For each of these separate analysis, we maintain the sponge geometry as
174 our base geometry and vary only the respective variable.

175 7.1. Rectangular Cross Section

176 This section shows the results when using a rectangular cross-section for the truss members. From fig. S10(a) it is
177 apparent that there exists an optimum for the diagonal separation that occurs when the spacing between diagonals are
178 approx 0.2 of the horizontal distance between vertical struts. This optimum value also persists when varying the loading
179 angle. From fig. S10(b) it can be seen that the linear stiffness is symmetrically and almost purely dependent on the mass
180 ratio allocated to diagonal versus non-diagonal elements. Comparing this figure to fig. S11(b) we can also see that even
181 the design cross-section does not change the linear stiffness behavior. fig. S10(c) shows that there exists two optimum
182 mass ratios, one where more material is allocated to the diagonal and one where there is more material allocated to
183 non-diagonals.

184 7.2. Circular Cross Section

185 For this cross-section we stay consistent with the natural sponge, and we can see from fig. S11 the overall behavior has
186 second order differences for (a), no change for (b) and a large difference in relative magnitude for (c). Furthermore, we
187 can see from the comparison between this section and section 7.1 that by using a rectangular cross-section we can tune
188 the mass ratio to achieve an overall structure with higher critical buckling strength.

189 8. LOCAL AND GLOBAL INSTABILITIES

190 ⇒ How should I go about describing this here?

191 9. STRESS CONCENTRATION

192 ⇒ add section on stress concentration for plane strain setting

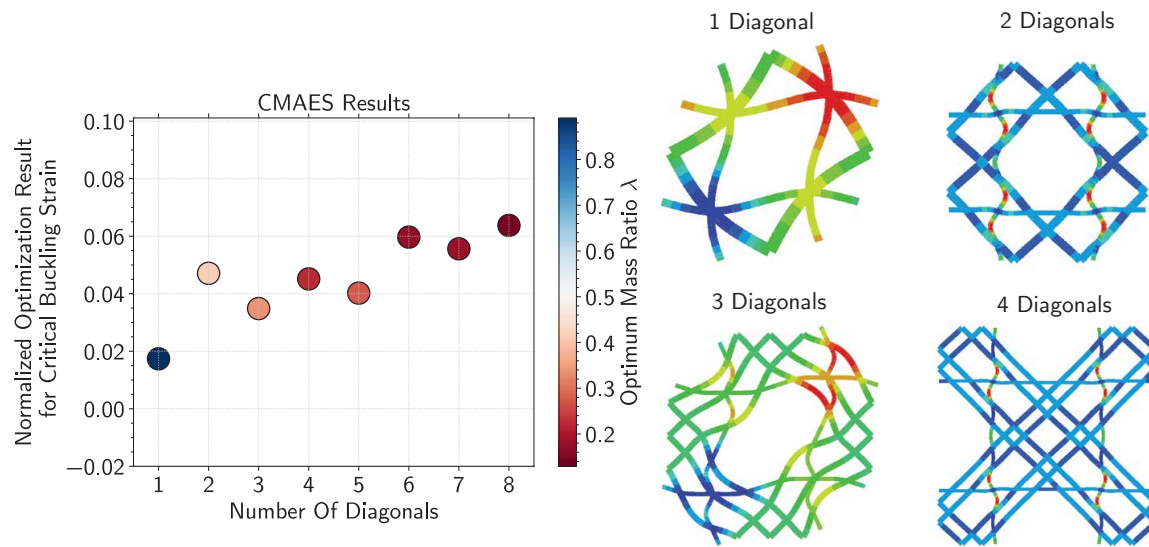


Figure S8: Buckling Optimization. Graph shows optimal value of critical buckling strain for varying number of diagonals. For all simulations, the total mass of the structure is maintained constant while the mass-ratio is allowed to vary. Furthermore, the diagonal separation for each pair of diagonal is allowed to vary together ensuring half symmetry of the structure at all times. The optimization is run under a uniaxial loading condition. The color of each point on the graph corresponds to the optimum value of mass ratio for that particular number of diagonals. Four deformation plots of the optimum structure and buckling modes are provided on the right for their respective number of diagonals.

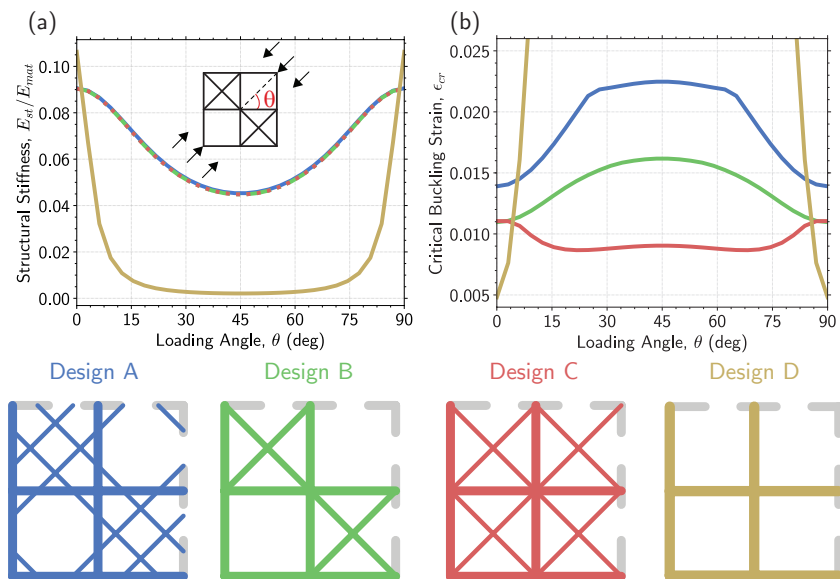


Figure S9: Circular Cross Section Results. The color of the lines correspond to its respective design color below the plots. (a) Shows the linear elastic stiffness of the different designs as a function of the loading angle. All structures except for the design without diagonal reinforcement have the same stiffness. (b) Shows the critical buckling strain for varying loading angle. For all angles, Design A outperforms other diagonally reinforced designs. These results show that the two diagonal benefit persists beyond a particular beam cross-section design.

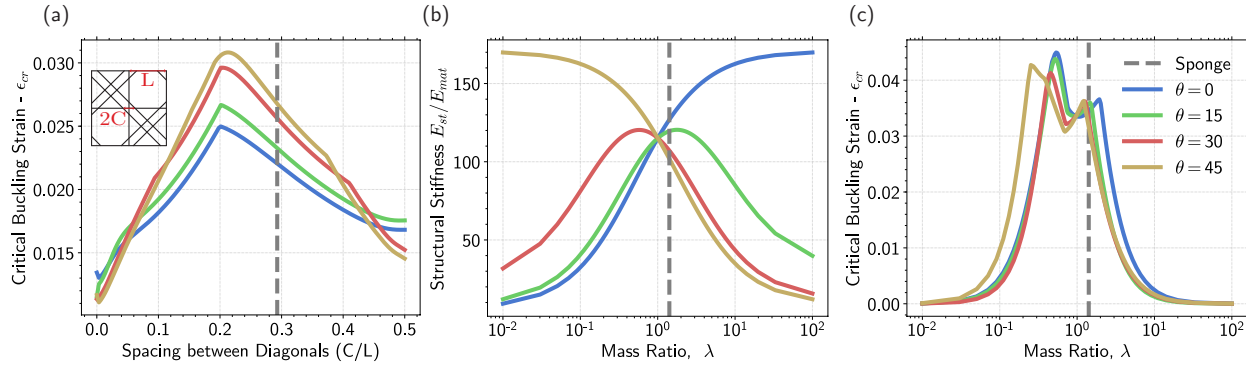


Figure S10: Rectangular Cross Section Parameter Exploration. For each of these plots, we vary a single parameter while maintaining the base sponge inspired geometry constant. The gray line indicates the sponge design parameter. (a) Shows the critical buckling strain for varying spacing between diagonals. (b) Shows the structural stiffness of the geometry as we vary the mass ratio λ . (c) Shows the critical buckling strain of the geometry as we vary the mass ratio λ .

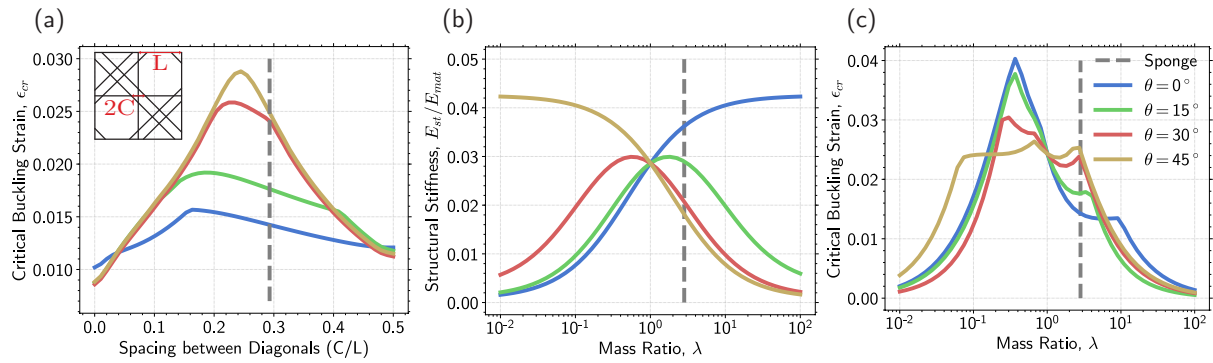


Figure S11: Circular Cross Section Parameter Exploration. For each of these plots, we vary a single parameter while maintaining the base sponge inspired geometry constant. The gray line indicates the sponge design parameter. (a) Shows the critical buckling strain for varying spacing between diagonals. (b) Shows the structural stiffness of the geometry as we vary the mass ratio λ . (c) Shows the critical buckling strain of the geometry as we vary the mass ratio λ .

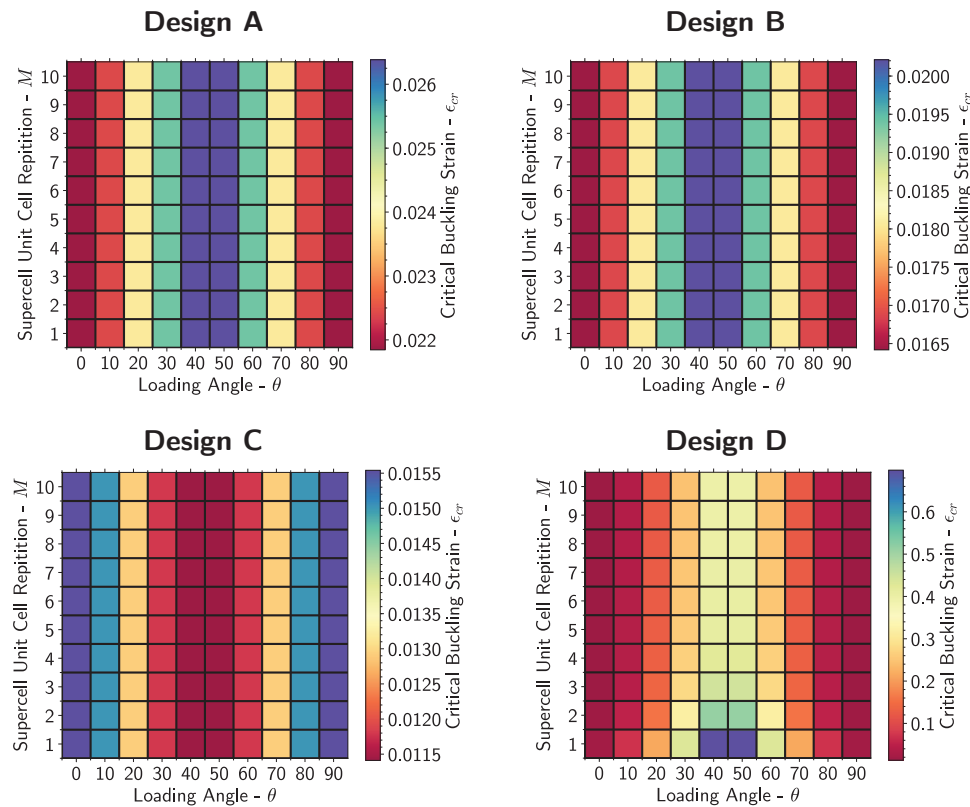


Figure S12: Global vs Local Instabilities. This figure shows four identical analysis performed on the Designs A-D. For each analysis we obtain the critical buckling strain for varying $M \times M$ tessellations (y-axis) of the unit cell also for varying loading angle θ (x-axis). The color of a pixel corresponds to a value of critical buckling strain for that simulation. For each of the simulations, periodic boundary conditions are applied along the outer perimeter of the $M \times M$ structure. This plot conveys that for Designs A-C the prominent buckling mode is the local mode, whereas for Design D, the prominent mode is a global mode. Choosing a sufficiently large M allows Design D to converge to a finite value for each θ .

193 REFERENCES

- 194 Joanna Aizenberg, James C Weaver, Monica S Thanawala, Vikram C Sundar, Daniel E Morse, and Peter Fratzl. Skeleton of euplectella sp.: structural hierarchy from the nanoscale to the macroscale. *Science*, 309(5732):275–278, 2005.
- 196 James C Weaver, Joanna Aizenberg, Georg E Fantner, David Kisailus, Alexander Woesz, Peter Allen, Kirk Fields, Michael J Porter, Frank W Zok, Paul K Hansma, et al. Hierarchical assembly of the siliceous skeletal lattice of the hexactinellid sponge euplectella aspergillum. *Journal of structural biology*, 158(1):93–106, 2007.
- 199 John Alexander Low Waddell. *Bridge engineering*, volume 1. J. Wiley, 1916.
- 200 Lorna J Gibson and Michael F Ashby. *Cellular solids: structure and properties*. Cambridge university press, 1999.
- 201 VS Deshpande, MF Ashby, and NA Fleck. Foam topology: bending versus stretching dominated architectures. *Acta Materialia*, 49(6):1035–1040, 2001.
- 203 M. Danielsson, D. M. Parks, and M. C. Boyce. Three-dimensional micromechanical modeling of voided polymeric materials. *Journal of Mechanics Physics of Solids*, 50:351–379, February 2002. .
- 205 K. Bertoldi and M. C. Boyce. Mechanically triggered transformations of phononic band gaps in periodic elastomeric structures. *Phys. Rev. B*, 77:052105, Feb 2008. . URL <https://link.aps.org/doi/10.1103/PhysRevB.77.052105>.
- 207 N. Hansen, S. D. Müller, and P. Koumoutsakos. Reducing the time complexity of the derandomized evolution strategy with covariance matrix adaptation (cma-es). *Evolutionary Computation*, 11(1):1–18, March 2003. ISSN 1063-6560. .